nature medicine

Myostatin is a direct regulator of osteoclast differentiation and its inhibition reduces inflammatory joint destruction in mice

Berno Dankbar[1], Michelle Fennen[1], Daniela Brunert[1], Silvia Hayer[2], Svetlana Frank[1], Corinna Wehmeyer[1], Denise Beckmann[1], Peter Paruzel[1], Jessica Bertrand[1], Kurt Redlich[2], Christina Koers-Wunrau[1], Athanasios Stratis[1], Adelheid Korb-Pap[1] & Thomas Pap[1]

Myostatin (also known as growth and differentiation factor 8) is a secreted member of the transforming growth factor-β (TGF-β) family that is mainly expressed in skeletal muscle, which is also its primary target tissue. Deletion of the myostatin gene (*Mstn*) in mice leads to muscle hypertrophy, and animal studies support the concept that myostatin is a negative regulator of muscle growth and regeneration[1–5]. However, myostatin deficiency also increases bone formation, mainly through loading-associated effects on bone[6–11]. Here we report a previously unknown direct role for myostatin in osteoclastogenesis and in the progressive loss of articular bone in rheumatoid arthritis (RA). We demonstrate that myostatin is highly expressed in the synovial tissues of RA subjects and of human tumor necrosis factor (TNF)-α transgenic (hTNFtg) mice, a model for human RA[12]. Myostatin strongly accelerates receptor activator of nuclear factor κB ligand (RANKL)-mediated osteoclast formation *in vitro* through transcription factor SMAD2-dependent regulation of nuclear factor of activated T-cells (NFATC1). Myostatin deficiency or antibody-mediated inhibition leads to an amelioration of arthritis severity in hTNFtg mice, chiefly reflected by less bone destruction. Consistent with these effects in hTNFtg mice, the lack of myostatin leads to increased grip strength and less bone erosion in the K/BxN serum-induced arthritis model in mice. The results strongly suggest that myostatin is a potent therapeutic target for interfering with osteoclast formation and joint destruction in RA.

Bone remodeling becomes disturbed in a variety of pathological conditions that affect the skeleton, including RA, in which there is local and/or systemic alteration in the levels of proinflammatory cytokines that are known to stimulate bone resorption *in vitro* and *in vivo*[13,14]. RA is the prototypic autoimmune disease primarily affecting the joints, and it is characterized by chronic inflammation and progressive cartilage and bone destruction[15]. Joints affected by RA usually lack signs of compensatory repair, which contributes to the rapid and progressive loss of joint structure. During the pathogenesis of RA, at the interface of the inflamed hyperplastic synovium and bone tissue, focal bone erosions occur, which are predominantly generated by osteoclasts[16–20]. Many of the cytokines and growth factors implicated in the chronic inflammatory process of RA have also been demonstrated to affect osteoclast differentiation[13,14,21]. In this context, TNF-α is a key cytokine in promoting bone destruction. It increases the number of bone-resorbing osteoclasts and decreases the number of bone-forming osteoblasts[22–25], thereby leading to an overall shift toward bone resorption.

Myostatin is a member of the TGF-β superfamily, several members of which have been implicated in bone turnover. However, the evidence that myostatin has a role in this context has been largely indirect[6–11]. To assess whether myostatin is involved directly in bone resorption and has a role in RA pathology, we first investigated the expression of myostatin *in vivo* as well as its regulation by inflammatory cytokines *in vitro*. Indeed, we observed high expression of myostatin in synovial membranes of patients with RA, with the most prominent staining of myostatin in synovial fibroblasts. In contrast, only very few myostatin-expressing cells were found in synovial tissues from control patients with osteoarthritis (OA) (**Fig. 1a**). In line with these results, expression of *MSTN* was identified in synovial fibroblasts obtained from subjects with RA (**Fig. 1b**) and higher levels of *MSTN* were also evident in synovial tissues from patients with RA compared to those with OA (**Fig. 1c**). These data suggested that the inflammatory environment of the synovium from people with RA leads to an upregulation of myostatin in synovial cells. We confirmed this hypothesis *in vitro*, where we found that stimulation of synovial fibroblasts from individuals with OA or those with RA with the recombinant inflammatory cytokines TNF-α, interleukin-1 (IL-1) and interleukin-17 (IL-17) resulted in higher expression of *MSTN*. The degree of stimulation compared to basal levels was approximately 1.7-fold, 1.8-fold and 3.0-fold, respectively, for the OA group and about 2.5-fold, 2.5-fold and 3.5-fold, respectively, for the RA group (**Fig. 1d**).

[1]Institute of Experimental Musculoskeletal Medicine (IEMM), University Hospital Muenster, Muenster, Germany. [2]Medical University of Vienna, Department of Internal Medicine III, Division of Rheumatology, Vienna, Austria. Correspondence should be addressed to T.P. (thomas.pap@uni-muenster.de).

Received 6 May; accepted 6 July; published online 3 August 2015; doi:10.1038/nm.3917

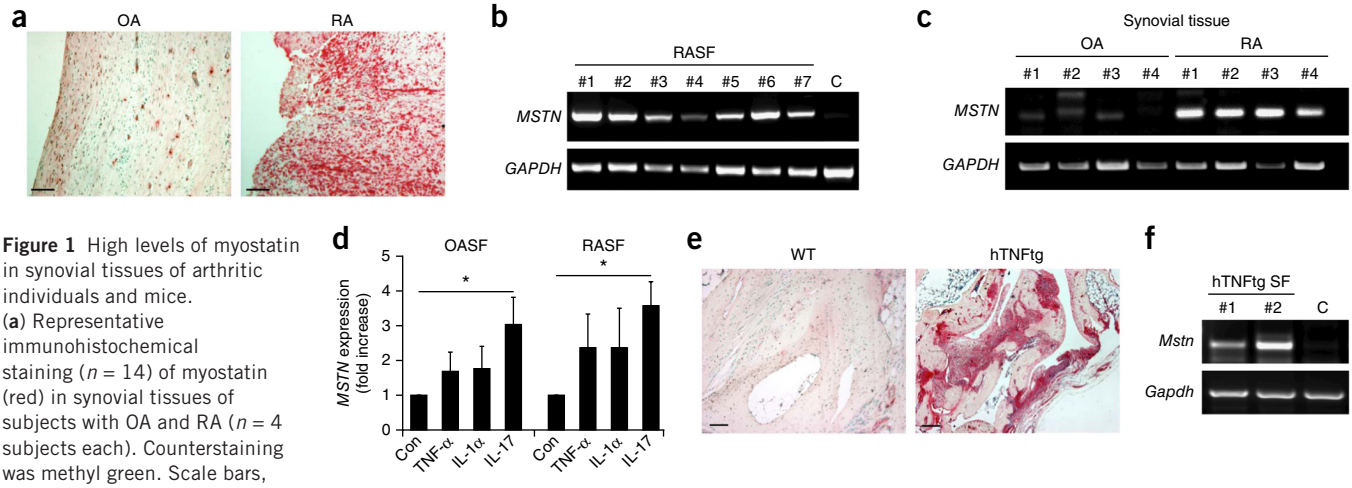

Figure 1 High levels of myostatin in synovial tissues of arthritic individuals and mice. (**a**) Representative immunohistochemical staining ($n = 14$) of myostatin (red) in synovial tissues of subjects with OA and RA ($n = 4$ subjects each). Counterstaining was methyl green. Scale bars, 200 µm. (**b**) Expression of *MSTN* in synovial fibroblasts (SF) of subjects with RA (RASF, $n = 7$). (**c**) Expression of *MSTN* in synovial tissues of subjects with RA compared to those with OA ($n = 4$ for each group). (**d**) Quantitative analysis of *MSTN* in OASF and RASF stimulated with various inflammatory cytokines. Con, unstimulated SF. Data show means ± s.e.m. of multiple measurements of two subjects with OA and three with RA. (**e**) Representative immunohistochemical staining ($n = 6$) of myostatin (red) in joint sections of WT and hTNFtg mice at 12 weeks of age ($n = 3$ mice each). Counterstaining was methyl green. Scale bars, 200 µm. (**f**) Expression of *Mstn* in synovial fibroblasts of hTNFtg mice (hTNFtg SF, $n = 2$). For gene expression analyses, glyceraldehyde-3-phosphate dehydrogenase (*GAPDH* or *Gapdh*) served as control. C, negative control. #, different human patients or mice. ns, not significant; $^*P < 0.05$; Kruskal-Wallis test with pairwise comparisons (**d**).

To further study whether chronic exposure to inflammatory factors results in upregulation of myostatin, we measured its expression in synovial membranes of hTNFtg mice, which develop a TNF-α–dependent chronic destructive arthritis[12]. We observed a strong expression of myostatin in synovial tissues of hTNFtg mice, whereas we found only negligible staining for myostatin synovial tissues of wild-type (WT, strain C57BL/6) mice (**Fig. 1e**), indicating that chronic inflammation leads to a sustained upregulation of myostatin. Again, expression of *Mstn* was detected in synovial fibroblasts of hTNFtg mice (**Fig. 1f**).

These findings prompted us to hypothesize that myostatin is involved in inflammatory bone destruction and raised the question of whether myostatin contributes directly to osteoclast-mediated bone resorption. Given that myostatin alone was not able to induce osteoclast formation of bone marrow–derived macrophages (BMMs) (**Fig. 2a**), we investigated the effects of myostatin on RANKL-induced osteoclastogenesis. Notably, the presence of myostatin significantly increased the ability of osteoclast precursors to differentiate into mature osteoclasts, reflected by a 3.8-fold higher number of osteoclasts after 4 d of differentiation in the presence of myostatin plus RANKL and macrophage colony-stimulating factor (M-CSF) compared to RANKL and M-CSF treatment alone (**Fig. 2a**).

Further, the conventional setting of osteoclast differentiation with M-CSF and RANKL alone generated only a few small osteoclasts during this short period of time (**Fig. 2a**). In contrast, we found that treatment of the cells with myostatin plus this conventional treatment resulted in very large osteoclasts with a huge cytoplasmatic compartment (eightfold greater compared to conventional treatment) and a very high number of nuclei (sevenfold greater compared to conventional treatment) (**Fig. 2b**). Notably, we found that myostatin did not influence the proliferation of apoptosis of treated BMMs (**Supplementary Fig. 1a**,**b**).

In line with these observations, BMMs obtained from myostatin-deficient mice ($Mstn^{-/-}$) showed a reduced RANKL-induced osteoclast formation *in vitro* (about 44% of WT BMMs) (**Fig. 2c**), and tibiae of $Mstn^{-/-}$ mice displayed lower osteoclast numbers of about 34%, compared to WT mice (**Supplementary Fig. 1c**), suggesting that myostatin-deficiency leads to a defect in osteoclast development. Accordingly, comparison of osteoclast morphologies revealed that osteoclasts from $Mstn^{-/-}$ mice were about one-third the size of osteoclasts from WT mice and contained about 50% fewer nuclei (**Fig. 2d**). As our BMM cultures are pure populations (confirmed by induction of cell death after M-CSF withdrawal; **Supplementary Fig. 1d**), these results strongly indicated an additional autocrine role of myostatin during osteoclast development. Finally, resorption pit analyses revealed a larger number of resorption pits formed by osteoclasts and a larger area overall from both WT and $Mstn^{-/-}$ mice in the presence of myostatin compared to RANKL treatment alone (**Fig. 2e**,**f**). Although pit numbers and overall resorption area were larger, no differences in resorption area per pit were detectable, indicating that myostatin has no effect on osteoclast activity *per se* (**Fig. 2f**).

As myostatin binds to and activates a heterodimeric complex of activin receptor 2B (ACVR2B) and ALK4 (officially known as ACVR1B) or ALK5 (officially known as TGFBR1)[26], we analyzed the expression of both myostatin and its receptors. Expression of myostatin in osteoclast precursors and mature osteoclasts but not in macrophages indicates that expression is induced by RANKL early in the differentiation process (**Fig. 2g**). The expression of myostatin and the identification of transcripts for ACVR2B and ALK4 and ALK5 in macrophages, osteoclast precursors and osteoclasts (**Fig. 2g**) further substantiate the hypothesis that myostatin is not only a paracrine stimulator of osteoclastogenesis but also an autocrine regulator of osteoclast formation. Moreover, co-culture experiments clearly showed that both the paracrine and autocrine actions of myostatin are important in the differentiation of osteoclasts. In particular, the lack of myostatin in BMMs cultured with WT osteoblasts led to a nearly 50% lower number of osteoclasts compared to co-cultures of WT BMMs and WT osteoblasts, whereas myostatin deficiency in osteoblasts resulted in a more than 90% lower number of osteoclasts after co-culture with WT BMMs, indicating that the paracrine action of myostatin is of critical importance (**Fig. 2h**).

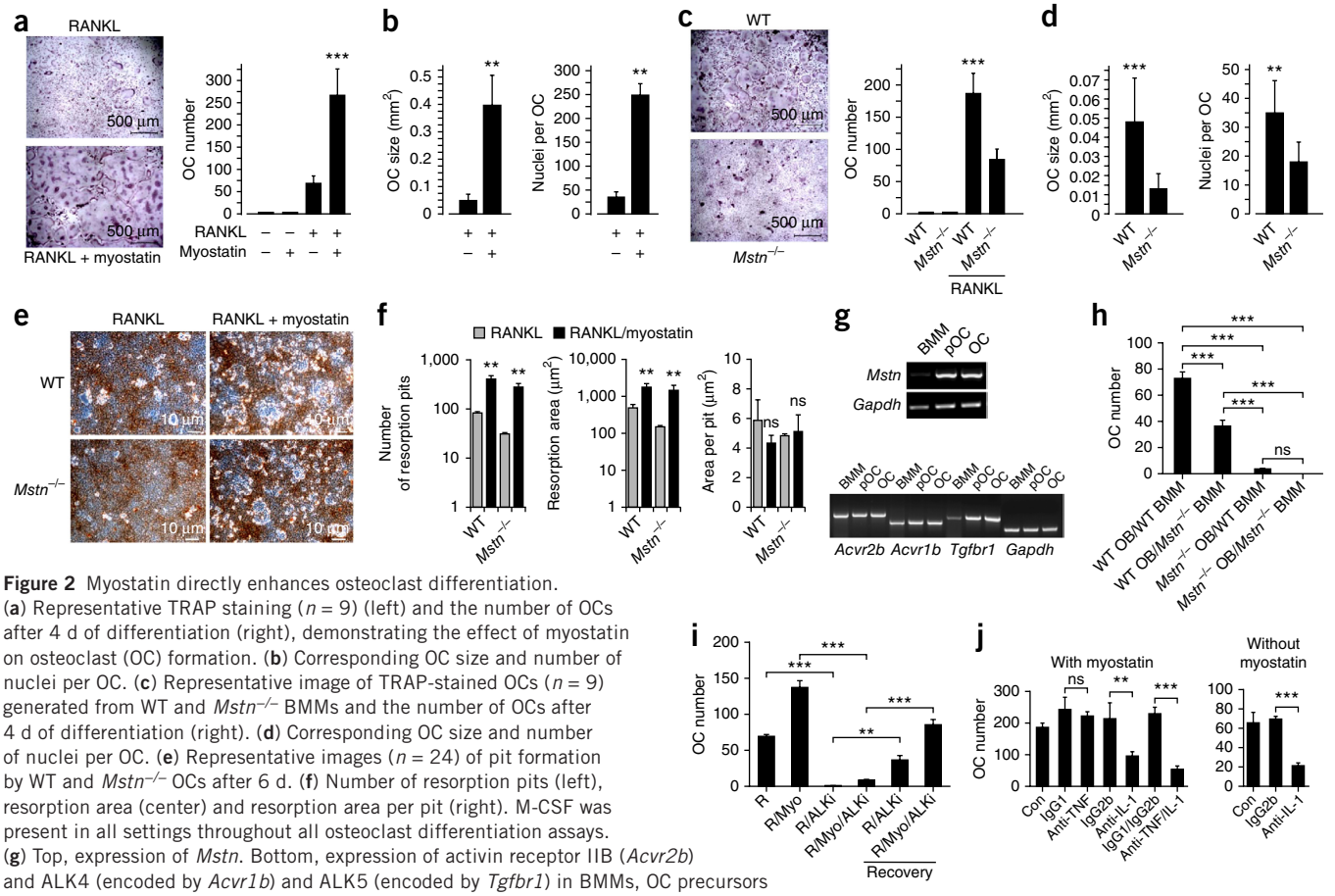

Figure 2 Myostatin directly enhances osteoclast differentiation. (**a**) Representative TRAP staining ($n = 9$) (left) and the number of OCs after 4 d of differentiation (right), demonstrating the effect of myostatin on osteoclast (OC) formation. (**b**) Corresponding OC size and number of nuclei per OC. (**c**) Representative image of TRAP-stained OCs ($n = 9$) generated from WT and *Mstn*$^{-/-}$ BMMs and the number of OCs after 4 d of differentiation (right). (**d**) Corresponding OC size and number of nuclei per OC. (**e**) Representative images ($n = 24$) of pit formation by WT and *Mstn*$^{-/-}$ OCs after 6 d. (**f**) Number of resorption pits (left), resorption area (center) and resorption area per pit (right). M-CSF was present in all settings throughout all osteoclast differentiation assays. (**g**) Top, expression of *Mstn*. Bottom, expression of activin receptor IIB (*Acvr2b*) and ALK4 (encoded by *Acvr1b*) and ALK5 (encoded by *Tgfbr1*) in BMMs, OC precursors (pOC) and mature OCs. *Gapdh* served as control. (**h**) Formation of OCs in co-cultures of osteoblasts with BMMs. (**i**) Inhibition of OC formation by a specific ALK4/5/7 inhibitor. (**j**) Effect of antibody-mediated TNF-α and IL-1 inhibition on OC formation. All data represent means ± s.e.m. of multiple measurements of at least three mice. ns, not significant; $^{**}P < 0.01$, $^{***}P < 0.001$. For **a** and **b** we used the Wilcoxon test; for **c**, **d**, and **f** we used the Mann-Whitney *U* test; and for **h**, **i**, and **j** we used the Kruskal-Wallis test with pairwise comparisons.

In addition, myostatin did not regulate expression of RANKL and M-CSF in mouse synovial fibroblasts and osteoblasts, suggesting that the paracrine action of myostatin on osteoclast formation is a direct effect (**Supplementary Fig. 1e**). We also found reduced osteoclast differentiation of BMMs after administration of a specific ALK4, ALK5, and ALK7 (officially known as ACVR1C) inhibitor compared to untreated differentiation controls (**Fig. 2i**), thereby confirming that the enhanced osteoclast formation is a receptor-mediated effect of myostatin. However, the ~90% lower number of osteoclasts suggests that in addition to myostatin, activin signaling, which has been shown to be important for osteoclast differentiation, may account for the ALK-inhibitory effects[27,28].

To explore whether autocrine actions of TNF-α and IL-1, both known to be important for osteoclastogenesis[29], are involved in myostatin-enhanced osteoclast development, we tested neutralizing antibodies against both cytokines. We found no inhibition of myostatin-enhanced osteoclast formation in the presence of a neutralizing TNF-α–specific antibody, but we observed a pronounced inhibition in the presence of a blocking IL-1 antibody. However, the IL-1 antibody also inhibited osteoclast development independently of myostatin (**Fig. 2j**), suggesting that an autocrine activity of IL-1 is indeed critical for osteoclastogenesis, but that it does not directly influence the stimulating effect of myostatin on this process.

These data prompted us to ask whether the loss of myostatin protects against bone damage during inflammatory destructive arthritis. To this end, we crossed hTNFtg mice, which develop a destructive RA-like disease[12,18], with *Mstn*$^{-/-}$ mice. Notably, clinical symptoms of arthritis occurred at less severity in hTNFtg;*Mstn*$^{-/-}$ mice compared to hTNFtg mice. *Mstn*$^{-/-}$ mice showed no clinical signs of arthritis. In particular, in hTNFtg;*Mstn*$^{-/-}$ mice paw swelling was delayed and occurred at about 66% of the degree observed in hTNFtg mice; this was accompanied by a higher grip strength of about 53% in the hTNFtg;*Mstn*$^{-/-}$ mice (**Fig. 3a**). In addition, hTNFtg;*Mstn*$^{-/-}$ mice showed significantly higher values of grip strength over time than hTNFtg mice, suggesting that structural damage is less pronounced in the absence of myostatin (**Fig. 3a**).

Because grip strength is influenced not only by arthritic joint damage but also by muscle mass and function, the possibility that the loss of myostatin influences this clinical parameter of arthritis through its effects on muscle cells cannot be excluded. However, microcomputerized tomography (microCT) and histomorphometric analyses showed a substantially reduced degree of joint destruction in arthritic mice lacking myostatin compared to the hTNFtg mice (**Fig. 3b**,**c**). Morphometric measurements confirmed less inflammation and bone erosion of 45% and 65%, respectively, compared to hTNFtg mice (**Fig. 3**). Moreover, the lower amount of bone erosion

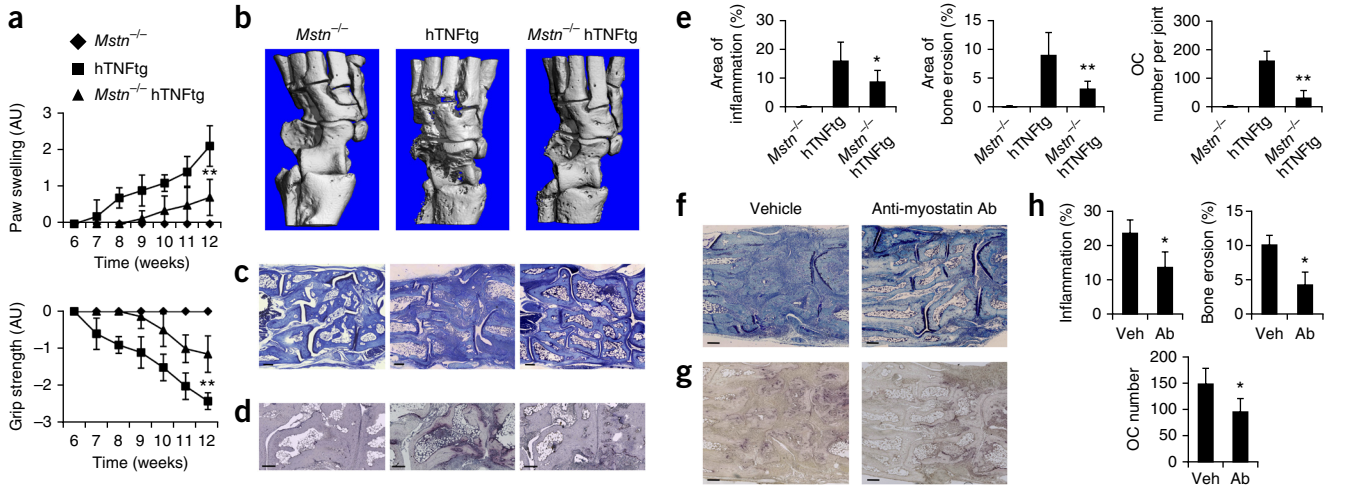

Figure 3 Deficiency or inhibition of myostatin ameliorates joint destruction in hTNFtg mice. (**a**) Effect of myostatin deficiency on paw swelling and grip strength in *Mstn*$^{-/-}$, hTNFtg, and hTNFtg;*Mstn*$^{-/-}$ mice over time. (**b**) Representative microCT ($n = 2$ per group) followed by 3D surface rendering of corresponding tarsal bones. (**c**) Representative microphotographs ($n = 5$ for *Mstn*$^{-/-}$;hTNFtg) and $n = 7$ for hTNFtg *Mstn*$^{-/-}$ mice) of corresponding toluidine blue–stained joint sections. (**d**) Representative TRAP stainings ($n = 5$ for *Mstn*$^{-/-}$;hTNFtg) and $n = 7$ for hTNFtg *Mstn*$^{-/-}$ mice) of corresponding joint sections. (**e**) Quantitative histomorphometric assessment of synovial inflammation, bone erosion, and osteoclast numbers in tarsal joints ($n = 5$ for *Mstn*$^{-/-}$;hTNFtg) and $n = 7$ for hTNFtg *Mstn*$^{-/-}$ mice). (**f,g**) Representative images of toluidine blue staining ($n = 8$) (**f**) and TRAP staining ($n = 8$) (**g**) of tarsal joint sections from hind paws of hTNFtg mice at week 12 treated subcutaneously with myostatin-specific antibody (Ab). (**h**) Corresponding quantitative histomorphometric analysis of inflammation and bone erosion and quantification of OC numbers in tarsal joints (four mice per group). Scale bars, 200 μm. All data represent means ± s.e.m. $^{*}P < 0.05$, $^{**}P < 0.01$. For **e** and **h** we applied the Mann-Whitney *U* test. AU, arbitrary units.

appeared to be a result of reduced osteoclast formation in myostatin-deficient arthritic mice (**Fig. 3d,e**).

In line with these data, treatment of hTNFtg mice with myostatin-specific antibody either intraperitoneally or locally in the hind paws led to a distinct improvement in disease severity. To analyze the effects on the occurrence of arthritic bone erosion, we initiated treatment at week 5, when hTNFtg mice exhibit the first histological signs of arthritis but do not yet exhibit full-blown disease[30]. We found that hTNFtg mice demonstrated fewer clinical signs, 10% less inflammation and 31% less bone erosion when treated intraperitoneally with myostatin-specific antibodies compared to vehicle-treated mice (**Supplementary Fig. 1f,g**). Amelioration of the disease was even stronger and nearly identical to that in the hTNFtg;*Mstn*$^{-/-}$ mice when the antibodies were administered subcutaneously into the hind paws of hTNFtg mice, as seen by ~42% less inflammation, 58% less bone erosion, and reduced osteoclast numbers by ~36% (**Fig. 3f–h**).

To evaluate whether reduced bone erosion is a result of reduced inflammation, we induced acute arthritis by using the K/BxN serum transfer model in *Mstn*$^{-/-}$ mice and WT mice. Of note, we again observed clearly less bone erosion associated with a lower number of osteoclasts (by about 50% and 60%, respectively) despite almost unaltered inflammation in the myostatin-deficient mice compared to the WT mice (**Supplementary Fig. 2a–d**). These results indicate that the observed reduction in bone erosion in arthritic myostatin-deficient mice is not a secondary effect of reduced inflammation.

To elucidate the mechanisms by which myostatin exerts its effect on osteoclast formation, we focused on the expression of the key differentiation markers integrin αv and integrin β3, c-src, NFATC1, DC-STAMP, ATP6V0D2, and calcitonin receptor in WT mice. Although RANKL induced the expression of all these differentiation markers, myostatin alone did not induce any of these markers (**Fig. 4a**). However, myostatin was clearly able to enhance RANKL-induced expression of integrin αv, integrin β3, DC-STAMP and calcitonin receptor during osteoclastogenesis, whereas no further increase of c-src and ATP6V0D2 was observed (**Fig. 4a**). As activation of the mitogen-activated protein kinase (MAPK) and nuclear factor-κB (NF-κB) pathways are key signaling events after RANKL stimulation in osteoclast precursor cells[31,32], we subsequently analyzed the effect of myostatin on these pathways. RANKL induced the phosphorylation of extracellular signal-regulated kinase 1/2 (ERK1/2), p38 MAPK-α (p38α), c-Jun N-terminal kinase (JNK), IκBα and NF-κB, but myostatin did not amplify RANKL-induced activation of the MAPK (**Fig. 4b**) or NF-κB (**Supplementary Fig. 2e,f**) pathways.

We next investigated whether, in turn, RANKL-mediated activation of ERK1/2 and p38, two MAPKs known to be essential for the development of osteoclasts[32,33], has any effect on myostatin-accelerated osteoclast formation. To this end, we used specific inhibitors of both MAPKs in the absence and presence of myostatin and studied RANKL-induced osteoclastogenesis. Without addition of myostatin, inhibition of both ERK1/2 and p38α resulted in a nearly complete inhibition of RANKL-mediated osteoclast formation, indicating that both MAPK pathways are indeed crucial for osteoclast development (**Fig. 4c**). Notably, and in contrast to inhibition of p38α, myostatin was potently able to counteract the consequences of ERK1/2 inhibition on osteoclast formation, suggesting that RANKL-induced and ERK-dependent target genes can be additionally activated by myostatin independently of ERK (**Fig. 4d**). In line with this notion, we found that RANKL-induced expression of NFATC1 and DC-STAMP, which was enhanced by myostatin, was reduced after ERK inhibition but remained high and unaffected in the presence of myostatin (**Fig. 4e**). Moreover, an increased activation of an NFATC1-luciferase reporter construct upon stimulation with RANKL and myostatin compared to RANKL alone confirmed that myostatin further activates NFATC1-dependent signaling pathways (**Fig. 4f**).

Because the increase in RANKL-induced NFATC1 expression in the presence of myostatin seemed to be independent of MAPK activation, we next wondered whether SMAD2, a known downstream signaling target of myostatin, mediates the observed effects on

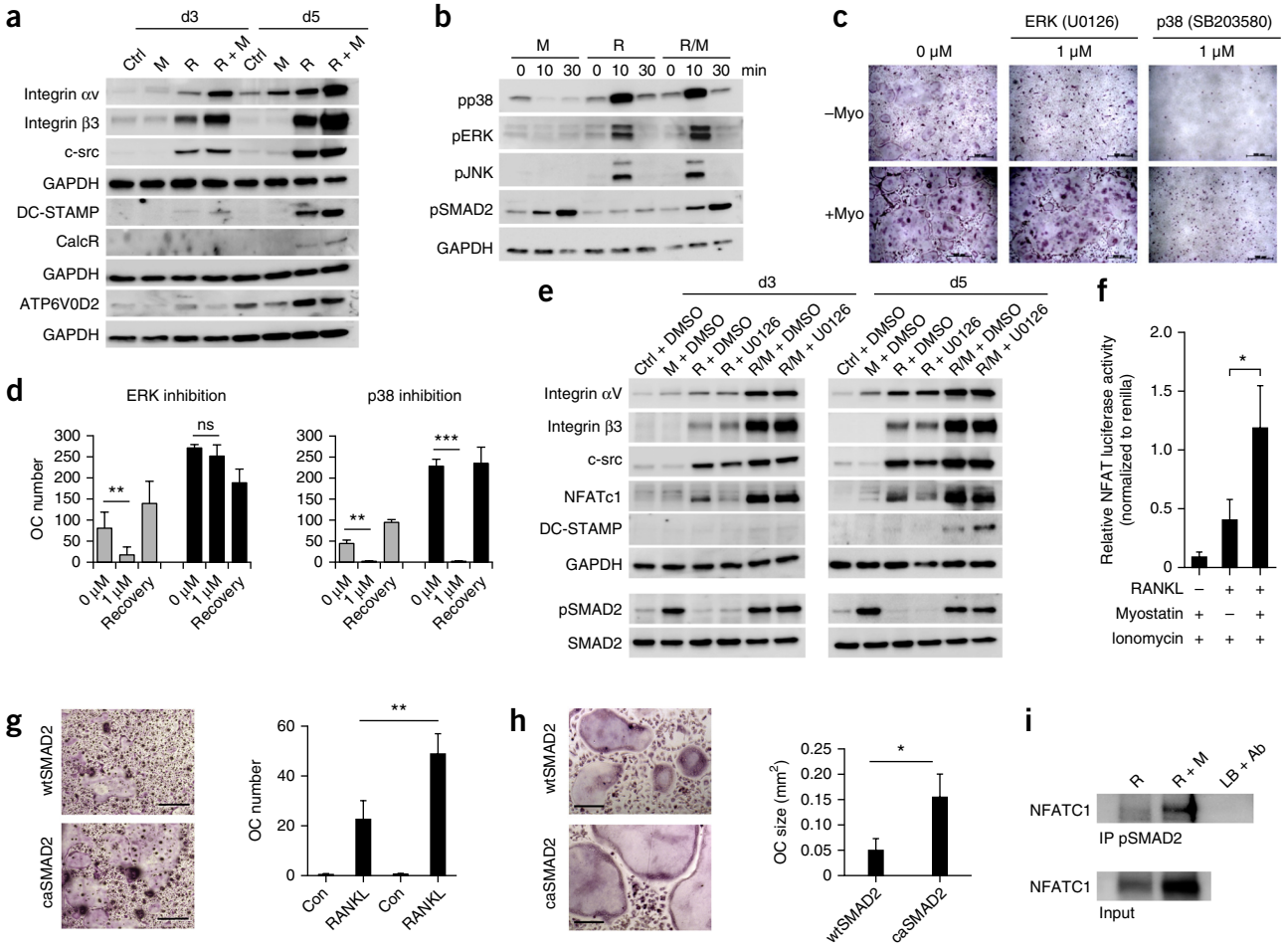

Figure 4 Myostatin enhances expression of key differentiation genes via SMAD2-dependent nuclear translocation of NFATC1. (**a**) Representative immunoblottings ($n = 34$) of OC differentiation markers upon stimulation of WT BMMs with RANKL (R), myostatin (M) or RANKL plus myostatin treatment for 3 and 5 d. ($n = 4$ mice). Ctrl, BMMs with M-CSF. GAPDH, loading control; CalcR, calcitonin receptor. (**b**) Representative immunoblottings ($n = 20$) of pp38MAPK ($n = 4$ mice), pERK1/2 ($n = 6$ mice), pJNK ($n = 4$ mice) and pSMAD2 ($n = 6$ mice) after stimulation of WT BMMs with myostatin, RANKL, or both at the indicated time points. (**c**) Representative TRAP stainings ($n = 36$) of OC formation after challenge with ERK (U0126) or p38MAPK (SB203580) inhibitors ($n = 3$ mice). Scale bars, 500 μm. (**d**) OC formation by RANKL (gray bars) or RANKL plus myostatin (black bars) after ERK and p38MAPK inhibition ($n = 3$ mice). (**e**) Representative immunoblottings ($n = 46$) of OC differentiation markers and SMAD2 activation upon stimulation of WT BMMs with myostatin, RANKL or RANKL + myostatin challenged either with or without 1 μM U0126 for 3 and 5 d ($n = 5$ mice). (**f**) Luciferase activity of RAW 264.7 cells transfected with pNFAT-Luc ($n = 3$ independent transfections). (**g**,**h**) Representative TRAP stainings ($n = 6$) of WT OCs transfected either with wtSMAD2 or caSMAD2 and (**g**) numbers of wtSMAD2 (gray bars) and caSMAD2 (black bars) transfected OCs and (**h**) corresponding OC size ($n = 3$ mice). Scale bars, 500 μm. (**i**) Co-Immunoprecipitation (IP) of pSMAD2 and NFATC1 in nuclear extracts from RANKL and RANKL + myostatin stimulated OC precursors ($n = 3$ mice). Lysis buffer (LB) plus antibody (Ab), negative control. All data show means ± s.e.m.; ns, not significant; $^*P < 0.05$, $^{**}P < 0.01$, $^{***}P < 0.001$. For **d** we used the Wilcoxon test; for **g** and **h** we used the Mann-Whitney *U* test.

osteoclastogenesis. Indeed, we found that Smad2 was consistently activated by myostatin (**Fig. 4b**). This activation occurred independently of RANKL-stimulation and was not influenced by the inhibition of ERK (**Fig. 4e**). These observations together led us ask whether the activation of Smad2 by itself would be sufficient to enhance RANKL-induced osteoclastogenesis. Indeed, transfection of BMMs with a constitutively active SMAD2 construct (caSMAD2) led to greater RANKL-induced osteoclast development by twofold compared to control (**Fig. 4g**) and osteoclast size (threefold compared to control, **Fig. 4h**).

In the light of a recent report suggesting a role for SMAD2 in the nuclear translocation of c-fos during RANKL-induced osteoclastogenesis[34], we finally studied a potential interaction of phosphorylated SMAD2 (pSMAD2) with NFATC1. Indeed, co-immunoprecipitation experiments showed that at co-stimulation of osteoclast precursor cells with RANKL and myostatin, NFATC1 was bound to pSMAD2 (**Fig. 4i**), suggesting that the effect of myostatin on osteoclast development is mediated by pSMAD2-dependent increased nuclear translocation of NFATC1.

In summary, we show that exposure of arthritic synovial fibroblasts to inflammatory cytokines results in a sustained upregulation of myostatin *in vitro* and *in vivo*. We further identified myostatin as an important direct paracrine and autocrine regulator of RANKL-induced osteoclast development *in vitro*. Myostatin exerts its effects through increased SMAD2-dependent nuclear translocation of NFATC1 and subsequent upregulation of osteoclast differentiation genes. Moreover, the loss or pharmacological inhibition of myostatin strongly reduces osteoclast formation and bone destruction in the hTNFtg mouse model of RA as well as in the serum-transfer-induced arthritis model. These data demonstrate that myostatin is critically

involved in osteoclast differentiation and bone destruction in RA, suggesting that myostatin may be a highly interesting pharmacological target for interfering with osteoclast formation and inflammatory joint destruction.

METHODS

Methods and any associated references are available in the online version of the paper.

Note: Any Supplementary Information and Source Data files are available in the online version of the paper.

ACKNOWLEDGMENTS

We thank S.-J. Lee (Johns Hopkins University School of Medicine) for providing us with the *Mstn*$^{-/-}$ mice, and G. Kollias (Alexander Fleming Biomedical Sciences Research Center) for the hTNF transgenic mice. We also thank Pfizer, Inc. for providing us with the myostatin-specific antibody. We thank X. Lin (Department of Surgery, Baylor College of Medicine) for providing us with the SMAD2 constructs. We thank V. Eckervogt and B. Truckenbrod for excellent technical support. This work was supported by the German Research Foundation (Deutsche Forschungsgemeinschaft; DA 1143/4-1 and DA 1143/4-2 to B.D. and T.P. as part of the Priority Programme SPP 1468, IMMUNOBONE) and by the Collaborative Research Center SFB 1009 granted to T.P.

AUTHOR CONTRIBUTIONS

B.D. designed and performed all experiments and wrote the manuscript; C.K.-W. and C.W. participated in the histomorphometric analyses; A.S., A.K-P. and P.P. contributed to experimental design and prepared mice and tissues and participated in the antibody experiments; D. Brunert performed the ELISA experiments and prepared mice; S.H. and K.R. conducted the studies with the K/BxN mouse model; S.F. participated in the transfection studies and performed the luciferase assays; M.F., J.B. and D. Beckmann performed the qPCR and the co-culture experiments; and T.P. participated in data analysis, directed the project and wrote the manuscript.

COMPETING FINANCIAL INTERESTS

The authors declare no competing financial interests.

1. McPherron, A.C., Lawler, A.M. & Lee, S.J. Regulation of skeletal muscle mass in mice by a new TGF-β superfamily member. *Nature* **387**, 83–90 (1997).
2. Huang, Z., Chen, X. & Chen, D. Myostatin: a novel insight into its role in metabolism, signal pathways, and expression regulation. *Cell. Signal.* **23**, 1441–1446 (2011).
3. Lin, J. *et al.* Myostatin knockout in mice increases myogenesis and decreases adipogenesis. *Biochem. Biophys. Res. Commun.* **291**, 701–706 (2002).
4. Wagner, K.R., Liu, X., Chang, X. & Allen, R.E. Muscle regeneration in the prolonged absence of myostatin. *Proc. Natl. Acad. Sci. USA* **102**, 2519–2524 (2005).
5. McCroskery, S. *et al.* Improved muscle healing through enhanced regeneration and reduced fibrosis in myostatin-null mice. *J. Cell Sci.* **118**, 3531–3541 (2005).
6. Kellum, E. *et al.* Myostatin (GDF-8) deficiency increases fracture callus size, Sox-5 expression, and callus bone volume. *Bone* **44**, 17–23 (2009).
7. Hamrick, M.W. *et al.* Loss of myostatin (GDF8) function increases osteogenic differentiation of bone marrow-derived mesenchymal stem cells but the osteogenic effect is ablated with unloading. *Bone* **40**, 1544–1553 (2007).
8. Hamrick, M.W. Increased bone mineral density in the femora of GDF8 knockout mice. *Anat. Rec. A Discov. Mol. Cell. Evol. Biol.* **272**, 388–391 (2003).
9. Hamrick, M.W., Pennington, C. & Byron, C.D. Bone architecture and disc degeneration in the lumbar spine of mice lacking GDF-8 (myostatin). *J. Orthop. Res.* **21**, 1025–1032 (2003).
10. Nicholson, E.K., Stock, S.R., Hamrick, M.W. & Ravosa, M.J. Biomineralization and adaptive plasticity of the temporomandibular joint in myostatin knockout mice. *Arch. Oral Biol.* **51**, 37–49 (2006).
11. Bialek, P. *et al.* A myostatin and activin decoy receptor enhances bone formation in mice. *Bone* **60**, 162–171 (2014).
12. Keffer, J. *et al.* Transgenic mice expressing human tumour necrosis factor: a predictive genetic model of arthritis. *EMBO J.* **10**, 4025–4031 (1991).
13. Goldring, S.R. Inflammatory mediators as essential elements in bone remodeling. *Calcif. Tissue Int.* **73**, 97–100 (2003).
14. Polzer, K. *et al.* Interleukin-1 is essential for systemic inflammatory bone loss. *Ann. Rheum. Dis.* **69**, 284–290 (2010).
15. Scott, D.L. *et al.* The links between joint damage and disability in rheumatoid arthritis. *Rheumatology* **39**, 122–132 (2000).
16. Goldring, S.R. Pathogenesis of bone erosions in rheumatoid arthritis. *Curr. Opin. Rheumatol.* **14**, 406–410 (2002).
17. Tsuboi, H. *et al.* Tartrate resistant acid phosphatase (TRAP) positive cells in rheumatoid synovium may induce the destruction of articular cartilage. *Ann. Rheum. Dis.* **62**, 196–203 (2003).
18. Redlich, K. *et al.* Osteoclasts are essential for TNF-α-mediated joint destruction. *J. Clin. Invest.* **110**, 1419–1427 (2002).
19. Schett, G. Cells of the synovium in rheumatoid arthritis. Osteoclasts. *Arthritis Res. Ther.* **9**, 203 (2007).
20. Suzuki, Y., Nishikaku, F., Nakatuka, M. & Koga, Y. Osteoclast-like cells in murine collagen induced arthritis. *J. Rheumatol.* **25**, 1154–1160 (1998).
21. Walsh, N.C., Crotti, T.N., Goldring, S.R. & Gravallese, E.M. Rheumatic diseases: the effects of inflammation on bone. *Immunol. Rev.* **208**, 228–251 (2005).
22. Li, P. *et al.* RANK signalling is not required for TNF-α-mediated increase in CD11^{hi} osteoclast precursors but is essential for mature osteoclast formation in TNF-α-mediated inflammatory arthritis. *J. Bone Miner. Res.* **19**, 207–213 (2004).
23. Lam, J. *et al.* TNF-α induces osteoclastogenesis by direct stimulation of macrophages exposed to permissive levels of RANK ligand. *J. Clin. Invest.* **106**, 1481–1488 (2000).
24. Ritchlin, C.T., Haas-Smith, S.A., Li, P., Hicks, D.G. & Schwarz, E.M. Mechanisms of TNF-α- and RANKL-mediated osteoclastogenesis and bone resorption in psoriatic arthritis. *J. Clin. Invest.* **111**, 821–831 (2003).
25. Bertolini, D.R., Nedwin, G.E., Bringman, T.S., Smith, D.D. & Mundy, G.R. Stimulation of bone resorption and inhibition of bone formation *in vitro* by human tumour necrosis factors. *Nature* **319**, 516–518 (1986).
26. Bradley, L., Yaworsky, P.J. & Walsh, F.S. Myostatin as a therapeutic target for musculoskeletal disease. *Cell. Mol. Life Sci.* **65**, 2119–2124 (2008).
27. Fuller, K., Bayley, K.E. & Chambers, T.J. Activin A is an essential cofactor for osteoclast induction. *Biochem. Biophys. Res. Commun.* **268**, 2–7 (2000).
28. Sugatani, T., Alvarez, U.M. & Hruska, K.A. Activin A stimulates IκB-α/NFκB and RANK expression for osteoclast differentiation, but not AKT survival pathway in osteoclast precursors. *J. Cell. Biochem.* **90**, 59–67 (2003).
29. Tani-Ishii, N., Tsunoda, A., Teranaka, T. & Umemoto, T. Autocrine regulation of osteoclast formation and bone resorption by IL-1 alpha and TNF alpha. *J. Dent. Res.* **78**, 1617–1623 (1999).
30. Korb-Pap, A. *et al.* Early structural changes in cartilage and bone are required for the attachment and invasion of inflamed synovial tissue during destructive inflammatory arthritis. *Ann. Rheum. Dis.* **71**, 1004–1011 (2012).
31. Lee, Z.H. & Kim, H.H. Signal transduction by receptor activator of nuclear factor kappa B in osteoclasts. *Biochem. Biophys. Res. Commun.* **305**, 211–214 (2003).
32. Lee, S.E. *et al.* The phosphatidylinositol 3-kinase, p38, and extracellular signal-regulated kinase pathways are involved in osteoclast differentiation. *Bone* **30**, 71–77 (2002).
33. Li, X. *et al.* p38 MAPK-mediated signals are required for inducing osteoclast differentiation but not for osteoclast function. *Endocrinology* **143**, 3105–3113 (2002).
34. Omata, Y. *et al.* Genome-wide comprehensive analysis reveals critical cooperation between Smad and c-Fos in RANKL-induced osteoclastogenesis. *J. Bone Miner. Res.* **30**, 869–877 (2015).

ONLINE METHODS

Human synovial tissues. All studies were approved by the ethics committees of the Medical University of the University Hospital Muenster. Samples of synovial tissues from subjects with RA or OA (according to the 1987 revised American College of Rheumatology criteria for RA and OA) were obtained at joint replacement surgery and provided by the Department of Orthopaedic Surgery, St. Joseph Hospital, Sendenhorst, Germany; by the Department of Orthopaedic Surgery of the University of Magdeburg School of Medicine, Magdeburg, Germany; and the Department of Orthopaedic Surgery, KMG-Kliniken Kyritz, Germany. All subjects gave informed consent prior to surgery.

Immunohistochemistry. Tissue samples from subjects with RA and OA as well as hind paws of *Mstn*$^{-/-}$, hTNFtg and hTNFtg;*Mstn*$^{-/-}$ mice were fixed in 4% paraformaldehyde overnight, embedded into paraffin and sectioned into 5 µm slices. We additionally decalcified mouse hind paws in 10% EDTA/TBS before paraffin embedding. Human and mouse tissue sections were pre-treated with 1× Trypsin/EDTA (PAA Laboratories, Pasching, Austria) for 15 min at 37 °C, blocked with 5% horse serum and stained with rabbit anti-human myostatin antibodies (NBP1-51196, Novus Biologicals, Cambridge, UK) overnight at 4 °C. We performed immunohistochemistry with an alkaline phosphatase technique using Vectastain ABC-A, Vector Red Substance and secondary biotinylated antibodies (Vector Laboratories, Burlingame, CA). Methyl green was used for counterstaining (Vector Laboratories, Burlingame, CA). Analyses were done in a non-blinded manner.

Fibroblasts and osteoblasts. We isolated human synovial fibroblasts by enzymatic digestion of synovial tissues using dispase II. Likewise, synovial fibroblasts from mice were isolated from deskinned dispase II digested hind paws. All cells were cultured in DMEM with 10% FCS at 37 °C and 5% CO_2. Initial contaminations with other cells (especially synovial macrophages) were eliminated by passaging of the cells. Human and mouse synovial fibroblasts were used between passages 4 and 7. Human synovial fibroblasts were challenged with hTNF-α (100 ng/ml, Peprotech, Hamburg, Germany), hIL-1α (20 ng/ml, R&D Systems, Nordenstadt, Germany), hIL-6/IL-6R (100 ng/ml, Peprotech), hTGF-β1 (20 ng/ml, R&D Systems) and IL-17 (20 ng/ml, R&D Systems) for 48 h and myostatin was assessed in supernatants by a commercial ELISA according to the manufacturer's recommendations (USCN Life Science, Hölzel Diagnostika, Cologne, Germany) or by qPCR. Mouse fibroblasts and osteoblasts (differentiated for 21 d, see co-cultures) were stimulated with 30 ng/ml myostatin for 48 h and MCSF and RANKL were determined in supernatants by ELISA according to the manufacturer's recommendations (R&D Systems, Nordenstadt, Germany).

RT-PCR and quantitative PCR. Total RNA was isolated from synovial tissues, cultivated synovial fibroblasts, bone marrow macrophages, and *in vitro* differentiated osteoclast precursors and osteoclasts using the RNeasy Mini kit (QIAGEN, Hilden, Germany). 1 µg total RNA was used for first strand cDNA synthesis (Life Technologies, Darmstadt, Germany) and 4 µl cDNA was then used for PCR using Taq-Polymerase (OmniBioLabs, Cologne, Germany) and the following primers: human myostatin (sense 5′-AGAGGGGCTGTGTAATGCATG-3′ and antisense 5′-GATGAGTCTCAGGATTTGCAC-3′ (427bp)), mouse myostatin[35], ACVR2B, ALK4, ALK5 (ref. 36), GAPDH[37]. Amplified transcripts of human *MSTN* and mouse *Mstn* were verified by sequencing (Sequiserve, Vaterstetten, Germany). For real-time PCR, samples of total RNA were reverse transcribed using a first strand cDNA synthesis kit (ThermoFisher Scientific, Schwerte, Germany). We performed amplification of the generated cDNA in a TaqMan 7300, using the following myostatin primer: sense 5′-AGGAGAAGATGGGCTGAATCCG-3′ and antisense 5′-AGAGGGTAACGACAGCATCGTG-3′ and the predesigned TaqMan gene expression primer Hs99999905_m1 for *GAPDH*, by following the manufacturer's guidelines (Applied Biosystems, Weiterstadt, Germany).

***In vitro* osteoclast generation and resorption assay.** For isolation of mouse BMMs from WT and *Mstn*$^{-/-}$ mice, femurs and tibias of 4–6-week-old mice were aseptically removed and BMMs were flushed out of the marrow cavity with α-MEM. Cells were cultured in α-MEM containing 10% FCS at 37 °C and 5% CO_2. We performed differentiation of BMMs by priming the cells with 50 ng/ml M-CSF for 72 h. After priming, we cultured the cells for further 4-6 days in the presence of M-CSF (50 ng/ml) and RANKL (50 ng/ml) with or without myostatin (30 ng/ml). All recombinant proteins were purchased from R&D Systems, Nordenstadt, Germany. Inhibition of autocrine TNF-α (ŢhMAB4101) and IL-1 (#MAB400) was achieved by incubation with neutralizing antibodies against TNF-α and IL-1 (25 µg/ml, R&D Systems, Nordenstadt, Germany) over the period of differentiation. For inhibition of myostatin-mediated receptor signaling, we used 1 uM of a specific ALK4/5/7 inhibitor[38] (SB431542, Sigma-Aldrich, Munich, Germany. For recovery of cells, inhibitors were removed and cells were differentiated for further 6 d. Inhibition of the MAPK p44/42 and p38 was achieved by administration of 1 µM U0126 (Cell Signaling, Frankfurt, Germany) and SB203580 (Merck, Darmstadt, Germany), respectively. We performed recovery experiments to assess toxicity of the inhibitors. For this purpose, inhibitors were removed after 5 d and washed cells were differentiated for further 4–6 d. Osteoclast formation was evaluated by TRAP staining (Leukocyte Phosphatase Staining Kit; Sigma-Aldrich, Munich, Germany). Resorption activity was evaluated by osteoclast-mediated pit formation on calcium phosphate-coated 24-well plates according to the manufacturer's recommendations (Cosmo Bio, Tokyo, Japan). For this, equal numbers of pre-fusion osteoclasts (72 h of differentiation with RANKL and with or without myostatin) were seeded onto the plates and further differentiated for 72 h.

Co-cultures. We performed co-culture experiments of BMMs and osteoblasts by seeding BMMs onto *in vitro*–differentiated osteoblasts. Mouse osteoblast precursors were isolated from calvaria of 3–5-d-old mice and differentiation was carried out by culturing the pre-osteoblasts in differentiation medium (MEM+Ham's F12 (1+1), 10% NBCS, L-ascorbate- 2-phosphate (0.2 mM), β-glycerolphosphate (10 mM), vitamin D3 (10 nM)) for 13 d. BMMs were seeded onto the osteoblast layer and cultured for 7 d in α-MEM containing 10% FCS, Prostaglandin E2 (1 µM) and vitamin D3 (10 nM). Osteoclast formation was assessed by TRAP staining.

Animals and treatments. Myostatin knockout mice[1] (*Mstn*$^{-/-}$) and human tumor necrosis factor α–transgenic mice (hTNFtg, Tg(TNF)197Gkl (ref. 12)), both on the C57BL/6 genetic background, were interbred to yield hTNFtg;*Mstn*$^{-/-}$ mice. All data were generated from age- and sex-matched female littermates at week 12 (except the inclusion of two male hTNFtg;*Mstn*$^{-/-}$ mice). Clinical signs of arthritis were determined once weekly as described previously[18] without blinding of the investigator. Female age-matched hTNFtg mice were randomized and treated with a neutralizing antibody against myostatin RK35 (ref. 39) either at an intraperitoneal dose of 50 mg/kg two times weekly or at a subcutaneous dose of 10 mg/kg two times weekly into hind paws or with PBS as control from week 5 to 12. Clinical signs of arthritis were determined once weekly with blinding of the investigator. Mice with serum transfer-induced arthritis were generated by injection of 8–10-week-old female *Mstn*$^{-/-}$ and WT control mice twice with 150 µl of arthritogenic serum from K/BxN mice (on day 0 and day 2; i.p.)[40]. Clinical symptoms of RA were documented every second or third day, beginning at day 4 after serum transfer. Paw swelling and grip strength was assessed in all four paws. Mice were killed on day 12 after serum transfer and both hind paws were prepared for histomorphometric analysis. Four-month-old WT and *Mstn*$^{-/-}$ mice were used for staining and quantification of osteoclasts in tibial heads. In all studies, no mice were excluded unless they died before the end of the study. All mouse procedures were approved by the local ethics committee 'Landesamt für Natur, Umwelt und Verbraucherschutz Nordrhein-Westfalen (LANUV)' (number: 8.87-51.05.2011.033; 84-02.04.2014.A132).

Micro-CT and histomorphometric analysis. We performed micro-CT on hind paws using MICRO-CT40 equipment (SCANCO-Medical, Switzerland). Serial decalcified paraffin-embedded sections (5 µm) of hind paws were stained with toluidine blue and TRAP for assessment of inflammation, bone erosion, and osteoclast numbers, respectively. We performed quantitative histomorphometric analysis on sections in a blinded manner using a Zeiss Observer.Z1 microscope and Zeiss AxioVision 4.8. software.

Immunoblotting. BMMs were cultured in the presence of 50 ng/ml M-CSF for 3 days. Cells were then stimulated with 50 ng/ml RANKL alone or in combination with 30 ng/ml myostatin for 0, 5, 10, 30, and 60 min. Cells were lysed in buffer containing 10 mM Tris, pH 7.4, 150 mM NaCl, 1 mM EDTA, 0.2% sodium deoxycholate, 1% NP-40, 1 mM NaF, 2 mM Na_3VO_4, and protease inhibitors (Roche Diagnostics, Mannheim, Germany). We performed western blotting with specific antibodies against integrin alpha-v (NBP1-96739, 1:1000, Novus Biologicals, Cambridge, UK), beta-3 (#4702, 1:1000) and Smad2 (#5339, 1:1000) (Cell Signaling, Frankfurt, Germany), c-src (AM00146PU-N, 1:1000, Acris, Herford, Germany), calcitonin receptor (250618, 1:100, Abbiotec, San Diego, USA), Atp6v0d2 (sc-69111, 1:200), DC-STAMP (sc-98769, 1:200), NFATc1 (sc-7294, 1:200) (all from Santa Cruz Biotechnology, Heidelberg, Germany) and the phosphorylated forms of p38α MAPK (#9211), ERK MAPK (#9101), JNK (#4668), Smad2 (#3101), IκBα (#2859) and NFκB (#3033) (all from Cell Signaling). For the purpose of control, blots were stripped and re-probed for GAPDH (#3683, 1:1000, Cell Signaling). All phospho-antibodies were used as 1:1000 dilutions.

Luciferase reporter assay. RAW 264.7 cells (mouse leukemic monocyte macrophage cell line) were transfected with the reporter plasmid, pNFAT-Luc (Agilent Technologies, Waldbronn, Germany) and *Renilla* luciferase vector (pRL-TK) control reporter vector (Promega, Mannheim Germany) using Lipofectamine2000 (Invitrogen). The pRL-TK plasmid, which expresses *Renilla* luciferase was used for normalization of transfection efficiency. After transfection for 6 h, we stimulated the cells with 50 ng/ml RANKL, 30 ng/ml myostatin or both for 17 h. Cells were harvested and their luciferase activities were measured using the dual luciferase reporter assay system (Promega).

Transfection of wtSMAD2 and caSMAD2. We performed transfection of wtSMAD2 and caSMAD2 (ref. 41) using jetPRIME (Polyplus-transfection, Illkirch, France) according to the manufacturer's instructions. *Wt* BMMs were incubated with 50 ng/ml M-CSF for 3 d, then transfected for 5 h and subsequently differentiated with 50 ng/ml RANKL for 7 d. Osteoclasts were stained by TRAP.

Co-immunoprecipitation. We performed co-immunoprecipitation using Dynabeads (Life Technologies) according to the manufacturer's protocol. Phospho-SMAD2 antibodies (Cell Signaling) were coupled to protein G–labeled Dynabeads. Equal amounts of nuclear extracts from BMMs differentiated with RANKL and RANKL+myostatin for 72 h were transferred to the pSMAD2 (#3101) antibody-bead complex and incubated for 1.5 h at room temperature. NFATC1 was subsequently detected by western blotting (sc-7294).

Assessment of cell viability, proliferation and apoptosis. For assessment of viability of BMM, cells were cultured with or without M-CSF or with M-CSF and myostatin for 72 h. Viability of BMMs was measured by the cellular reduction of 3-(4,5-dimethylthiazol-2-yl)-2,5-diphenyltetrazolium bromide (MTT-test). We assessed the influence of myostatin on proliferation of BMMs by counting the cells after culture in the presence of 50 ng/ml M-CSF and various concentrations of myostatin for 72 h. Apoptotic cell death of osteoclasts was quantified using the cell death detection ELISA (Roche Diagnostics) according to the manufacturers' instructions. We evaluated apoptosis by using *in vitro*–differentiated osteoclasts obtained by administration of 30 ng/ml M-CSF and 50 ng/ml RANKL with or without 30 ng/ml myostatin for 5 d. Administration of M-CSF and myostatin alone served as controls.

Statistical analysis. No statistical method was used to predetermine sample size. Rather, sample size was based on preliminary data and observed effect sizes. We performed statistical analysis using GraphPad Prism Software, 4.0 (Graph Pad Software Inc., San Diego, CA). If the normal distribution was not valid, statistical significance was evaluated using the Mann-Whitney rank-sum test (two-tailed) for differences between two independent groups and the Wilcoxon matched-pair signed-rank test (two-tailed) for comparison of differences within pairs. Statistical significance of overall differences between multiple groups was analyzed by the Kruskal-Wallis one-way analysis of variance. If the test was significant, pairwise comparisons were done by the multiple comparisons criterion. A value of $P < 0.05$ was considered statistically significant.

35. Li, Z.B., Kollias, H.D. & Wagner, K.R. Myostatin directly regulates skeletal muscle fibrosis. *J. Biol. Chem.* **283**, 19371–19378 (2008).
36. Machida, H., Ogawa, K., Funaba, M., Mizutani, T. & Tsujimoto, M. mRNA expression of type I and type II receptors for activin, transforming growth factor-beta, and bone morphogenetic protein in the murine erythroleukemic cell line, F5-5.fl. *Eur. J. Endocrinol.* **143**, 705–710 (2000).
37. Kaneto, H. *et al.* Increased expression of TGF-β1 but not its receptor contributes to human obstructive nephropathy. *Kidney Int.* **56**, 2137–2146 (1999).
38. Inman, G.J. *et al.* SB-431542 is a potent and specific inhibitor of transforming growth factor-beta superfamily type I activin receptor-like kinase (ALK) receptors ALK4, ALK5, and ALK7. *Mol. Pharmacol.* **62**, 65–74 (2002).
39. Holzbaur, E.L. *et al.* Myostatin inhibition slows muscle atrophy in rodent models of amyotrophic lateral sclerosis. *Neurobiol. Dis.* **23**, 697–707 (2006).
40. Monach, P.A., Mathis, D. & Benoist, C. The K/BxN arthritis model. *Curr. Protoc. Immunol.* **81**, 15.22.1–15.22.12 (2008).
41. Martinez, G.J. *et al.* Smad2 positively regulates the generation of Th17 cells. *J. Biol. Chem.* **285**, 29039–29043 (2010).

doi:10.1038/nm.3917